JOURNAL OF AGRICULTURAL AND FOOD CHEMISTRY

pubs.acs.org/JAFC Article

DNA-Gated Graphene Field-Effect Transistors for Specific Detection of Arsenic(III) in Rice

Yuhong Wang, Yulong Bi, Rongrong Wang, Lu Wang, Hao Qu,* and Lei Zheng

Cite This: J. Agric. Food Chem. 2021, 69, 1398−1404 Read Online

ACCESS | Metrics & More | Article Recommendations | Supporting Information

ABSTRACT: As one of the most toxic forms of arsenic, inorganic As(III) is easy to accumulate in rice, leading to severe public health problems. Effective control of As(III) requires the development of fast analytical methods for its detection with high sensitivity and specificity. Toward this end, in this work, we report the fabrication of an As(III) electrochemical sensor based on a solution-gated graphene transistor (SGGT) platform with a novel sensing mechanism. The gold gate electrode of the SGGT was modified with DNA probes and then blocked with bovine serum albumin (BSA). The specific interaction between As(III) and gold disrupted the adsorption states of DNA probes, redistributing surface charges on the gate electrode, further leading to potential drop changes at the interfaces of the gate electrode and graphene active layer. This new mechanism based on DNA-charge-redistribution-induced SGGT current responses (denoted as "DNA-SGGT") was found to greatly improve the selectivity of the sensor: the response of DNA-SGGT to As(III) was effectively enhanced fourfold, while to other interfering cations, it was significantly reduced. The optimized sensor showed a detection limit as low as 5 nM with superior selectivity to As(III). The as-prepared DNA-SGGT-based sensor has also been successfully applied to the detection of As(III) in practical rice samples with a high recovery rate, showing great potential for heavy metal detection in many types of food samples.

KEYWORDS: *arsenic, rice, DNA-gated graphene transistor, biosensor, electrochemistry*

INTRODUCTION

Rice is the main food supply for more than half of the world's population, so the quality of rice is concerned to hundreds of millions of people.[1] Compared with other cereal crops, rice crops accumulate arsenic much more efficiently,[2,3] resulting in higher arsenic levels.[4] Sites of contamination are found worldwide as a result of both natural processes and anthropogenic activities.[5] Arsenic-rich rice may cause high risks for public health since it is one of the first chemicals designated as a group I carcinogen,[6] and it has been widely recognized that chronic exposure to it may lead to serious effects on human health for many years. It mainly enters the human body through the digestive tract and respiratory tract[7] and then scatters in many tissues and blood in the body, causing extreme difficulties for its removal.[8] For these reasons, the US FDA has regulated that the upper limit of arsenic in rice is 0.12 mg/kg. In the environment, As mainly exists in its inorganic forms, arsenate [As(V)] and arsenite [As(III)],[9,10] between which As(III) is 60 times more toxic than As(V) or other organic As compounds.[11] Therefore, it is of more significance to monitor As(III) concentration.[12]

Currently, the commonly used methods for arsenic detection are chromatography and spectroscopy,[13] such as high-performance liquid chromatography (HPLC),[14−16] ion chromatography (IC),[17] gas chromatography (GC),[18] inductively coupled plasma-mass spectrometry,[19] and atomic fluorescence spectrometry.[20,21] However, these methods have many limitations in practical applications. For example, they generally require large equipment, complex operation, and excessive maintenance costs and are time-consuming.[22] Toward this end, many fast detecting methods, such as electrochemistry-based,[23] surface-enhanced Raman scattering assays,[24] surface plasmon resonance sensors,[25] chemosensors,[23] and biosensors,[26] have also been developed recently. Among them, electrochemical sensors that measure direct current responses have attracted broad attention for being simple, flexible, and easily automated for routine analysis.[27]

Single-layer graphene has been obtained via the physical exfoliation method.[28,29] In the last decade, single-layer graphene-based field-effect transistors have drawn a lot of interests due to the excellent properties of graphene, such as high electrical conductivity, excellent physical properties, massless carriers (both electrons and holes), high transparency, and extremely high carrier mobility.[30−32] Among them, solution-gated graphene transistors (SGGTs) have been applied for detection of many types of analytes, such as DNA,[33] pH variation,[34] glucose,[35] and metal ions (including K^+,[36] Na^+,[37] etc.) with extremely high sensitivity due to the inherent signal amplification. Our previous studies have shown that SGGTs have also great potential for practical applications in detection of hazardous components in food samples for food safety inspection purposes.[38−40] However, when used as ion sensors, one of the greatest limitations for SGGTs is lack of

Received: November 8, 2020
Revised: December 31, 2020
Accepted: December 31, 2020
Published: January 12, 2021

https://dx.doi.org/10.1021/acs.jafc.0c07052
J. Agric. Food Chem. 2021, 69, 1398−1404

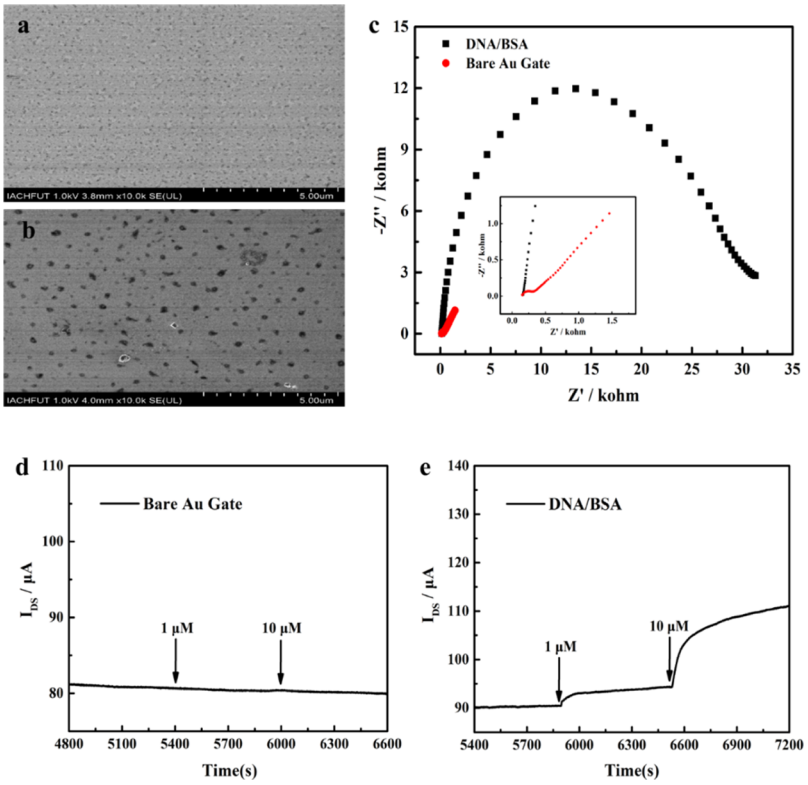

Figure 1. Characterization of the DNA/BSA-modified gate electrode. The SEM images of the (a) bare Au gate and (b) DNA/BSA-modified gate. (c) EIS of the bare Au gate (red dots) and DNA/BSA-modified gate (black squares). Real-time current responses for continuous addition of cDNAs for the (d) SGGT with the bare Au gate and (e) DNA-SGGT with DNA/BSA-modified gate electrodes.

selective response to a specific ion, since the detection mechanism is solely the change in dirac point voltages (V_{dirac}) of the devices induced by nonspecific electrochemical reactions of ions at the gate[36,38] or changes in electrolyte conditions by these ions.[41,42]

Toward this end, in this work, we report the fabrication of an As(III)-sensor based on the DNA-modified SGGT with a novel detection mechanism for enhanced sensitive and selective responses. First, the SGGT gate electrode was modified with DNA oligonucleotides, and the remaining surface sites were blocked with bovine serum albumin (BSA). We found that the surface charge redistribution of the gate electrode caused by the disruption of the interaction between DNA probes and the gold surface specifically by As(III) ions[43,44] may also lead to changes in electric double layers (EDLs) at interfaces and thus significant channel current responses. Although there has been little pioneer work to improve the specificity of SGGTs to Pb^{2+} ions by modifying the graphene channel with DNAzymes,[45] this is the first report about the application of the new sensing mechanism of SGGTs with current response induced by GATE surface charge redistribution regulated by DNA probes, denoted as the "DNA-gated field-effect graphene transistor" (DNA-SGGT). The optimized DNA-SGGT sensor showed an enhanced (by fourfold) channel current response to As(III), while that to other interfering cations was significantly suppressed, with a detection limit as low as 5 nM and superior selectivity to As(III). Finally, we also applied the DNA-SGGT-based sensor for the detection of As(III) in practical rice samples and obtained high recovery rates.

EXPERIMENTAL SECTION

Materials. As_2O_3 was purchased from Xiya Reagent (Shandong, China). The DNA sample was synthesized by Sangon Biotech (Shanghai) with HPLC purification. Phosphate-buffered saline (1× PBS, a mixed solution of 8 mM Na_2HPO_4, 136 mM NaCl, 2 mM KH_2PO_4, and 2.6 mM KCl, with pH = 7.2), tris-(2-carboxyethyl)-phosphine hydrochloride (TCEP), acetone, isopropanol, and ethanol were purchased from Sangon Biotech (Shanghai, China). Tris-HCl buffer (pH 8.0) was purchased from Solarbio. BSA, potassium chloride (KCl), sodium chloride (NaCl), magnesium chloride ($MgCl_2$), and other selective interfering compounds were all obtained from Sinopharm (Shanghai, China). The arsenic-free rice was purchased from a local Metro supermarket. Ultrapure deionized (DI) water obtained from the Milli-Q system (18.2 MΩ, Millipore, Bedford, MA, USA) was used throughout the research. Other common reagents were used without further purification.

Preparation of SGGT Electrodes. The glass slides (1 cm × 1.2 cm) were rinsed three times with acetone, isopropanol, ethanol, and then DI water successively under ultrasonic conditions. The glass substrate was blow-dried with high-purity nitrogen and then glued to the mask plate with high-temperature tape, and the slide surface was plated with 10 nm patterned Cr/Au source, drain, and gate electrodes by magnetron sputtering. Monolayer graphene layers were synthesized by chemical vapor deposition (CVD)[29] of CH_4 (40 SCCM) and H_2 (20 SCCM) using 25 μm-thick copper foil as a catalytic substrate at 1000 °C. Prior to graphene transfer, the substrate surface was treated with O_2 plasma for 6 min to enhance hydrophilicity. A polymethyl methacrylate (PMMA) film was spun onto graphene, and the graphene/PMMA was transferred to the channel area. The sensor was annealed at 120 °C for 15 min and soaked in acetone at 55 °C for 1 h and washed three times to remove PMMA. Finally, the sensor was sealed with waterproof glue and silver paste to avoid direct contact with the electrolyte during the characterization process.

Preparation of DNA-Modified Electrodes. The SGGT sensor was rinsed three times with 1× PBS to ensure a clean surface before

https://dx.doi.org/10.1021/acs.jafc.0c07052
J. Agric. Food Chem. 2021, 69, 1398−1404

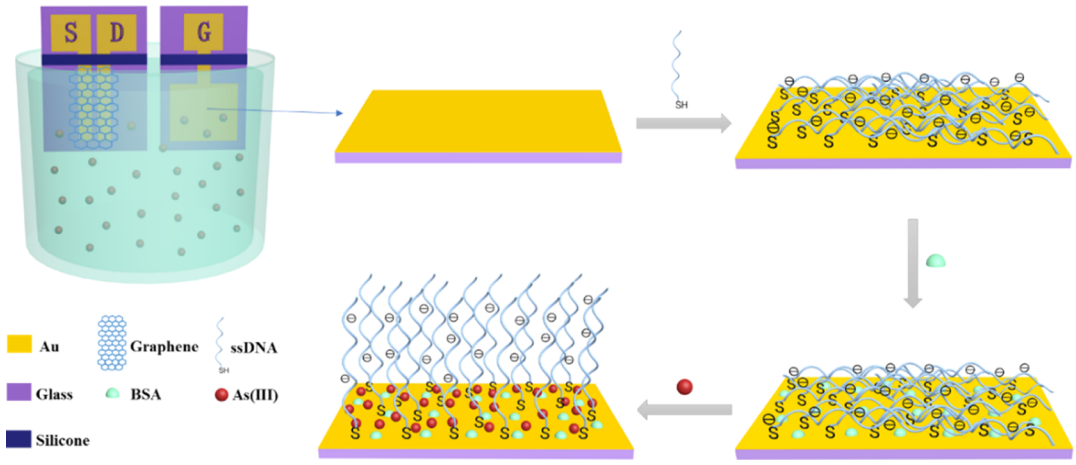

Figure 2. Schematic diagram As(III) detection using the DNA-SGGT with the DNA/BSA-modified gate. The sensor consists of source, drain, and gate electrodes and a graphene channel. The gate electrode was functionalized with single-stranded DNA and then blocked with BSA. Before the addition of As(III), the DNA strands were adsorbed on the gate. The interaction between As(III) ions and Au interrupts this DNA adsorption and hence changes the states of DNA probes on the gate electrode, causing significant changes in surface charge distribution of the gate.

all modifications and tests. In order to modify the DNA onto the bare Au gate electrode, we synthesized DNA with thiol modification at the 5′ end, that is, the (5′−HS−S−$(CH_2)_6$−GGT AAT ACG ACT CAC TAT AGG GAG ATA CCA GCT TAT TCA ATT TTA CAG AAC AAC CAA CGT CGC TCC GGG TAC TTC TTC ATC GAG ATA GTA AGT GCA ATC T-3′) sequence for self-assembly of the DNA strand to the Au electrode surface. The DNA probe was freshly reduced by mixing 1 μM of the probe with 10 μM TCEP in Tris-HCl buffer (10 mM, pH 8.0) containing 1.0 M NaCl for 1 h. The cleaned Au electrode was then immersed in the abovementioned solution for 12 h at room temperature. After that, the electrode was incubated in 10 mg/mL BSA solution for 30 min for electrode blocking. Finally, the electrode was rinsed thoroughly with Tris-HCl buffer containing 0.5 M NaCl three times.

Device Characterization and Electrochemical Measurement. The electrochemical properties of the bare and modified electrodes were characterized by the CHI650D electrochemical workstation (Shanghai CH Instruments Inc., China). The traditional three electrodes, consisting of bare Au or the DNA-modified electrode, platinum wire as the counter electrode, and saturated calomel electrode as the reference electrode, were tested. Electrochemical impedance spectroscopy (EIS) was performed on the bare Au gate and DNA-modified gate in 0.1 mM KCl solution containing 5.0 mM $[Fe(CN)_6]^{3-/4-}$ and the frequency range from 0.1 to 10^5 Hz, and the potential used was 0.2 V.[46]

Before measurement, all devices were soaked in 1× PBS for 15 min to remove surface residues from the electrodes and graphene channel. The DNA-SGGT-based As(III) sensor, consisting of source, drain, and gate electrodes, was tested for performance in a small beaker containing 10 mL of phosphate buffer (1× PBS, pH = 7.4). The source, drain, and gate were connected to two source meters (Keithley 2400), and the gate voltage (V_G) and source drain voltage (V_{DS}) were controlled using a customized LabVIEW program (see Figure S1 for more details). Different concentrations of As(III) were added to PBS to obtain successive different I_{DS} responses. The transfer characteristic curve (I_{DS}−V_G) was measured with the channel current between the source and drain as a function of V_G under a fixed source−drain voltage V_{DS} = 0.05 V and different gate voltages V_G: 0−0.8 V and a scanning rate of 0.01 V/s. The channel current and time curve (I_{DS}−t) under a fixed source−drain voltage V_{DS} = 0.05 V and constant gate voltage V_G = + 0.7 V and the current response of the sensor I_{DS} to different concentrations of As(III) was recorded over time.

The detection method and conditions for complementary DNA (cDNA) with the sequence shown in Table S1 at different concentrations were the same as described above.

RESULTS AND DISCUSSION

Characterization of DNA/BSA-Modified Electrodes. Figure 1a,b shows the scanning electron microscopy (SEM) images of the gate electrode surface before and after the DNA modification and BSA blocking. The obvious change (black dots) indicates the success of the functionalization with the DNA and BSA. Next, we conducted EIS measurements to characterize the impedance change induced by functionalization, and the results are shown in Figure 1c. It can be seen that the Nyquist plots of the two electrodes show a clear semicircle at high frequencies, the diameter of which generally reflects the interfacial charge transfer resistance (R_{ct}).[46] From Figure 2c, it was observed that the R_{ct} value of the bare Au electrode was 1.5 KΩ, while that of the modified electrode was 30 KΩ. The significant increase in R_{ct} value also suggested that the gate electrode was effectively modified by DNA probes and BSA.

For further evaluation of the DNA/BSA modification of the gate electrode, we applied the fabricated DNA-SGGT sensor to measurement of DNA strands that were complementary to the DNA probes (cDNA), as depicted in Figure S3. For the SGGT with the bare Au gate electrode, the addition of cDNA did not induce obvious current response, as shown in Figure 1d. In contrast, for the DNA-SGGT with the DNA/BSA-modified gate electrode, when cDNA was added, strong channel current response was observed (as shown in Figure 1e), attributed to the change in surface charges at the gate electrode induced by the hybridization of cDNA strands. This measurement also confirmed the success of modification with DNA probes. Moreover, more importantly, it gave us the implication of a novel detection mechanism for the SGGT that the surface charge changes may also cause obvious channel current responses through the field-effect amplification, which was used for subsequent As(III) detection.

Detection Mechanism of the DNA-SGGT-Based As(III) Sensor. As sketched in Figure 2, the established DNA-SGGT-based As(III) sensor was composed of three electrodes (i.e., source, drain, gate electrodes) and a graphene channel. Both the gate electrode and graphene channel were in contact with electrolyte solution to form two EDLs, as shown in Figure S2. When the SGGT works in both p-type and n-type domains, the channel current can be described by[47]

https://dx.doi.org/10.1021/acs.jafc.0c07052
J. Agric. Food Chem. 2021, 69, 1398−1404

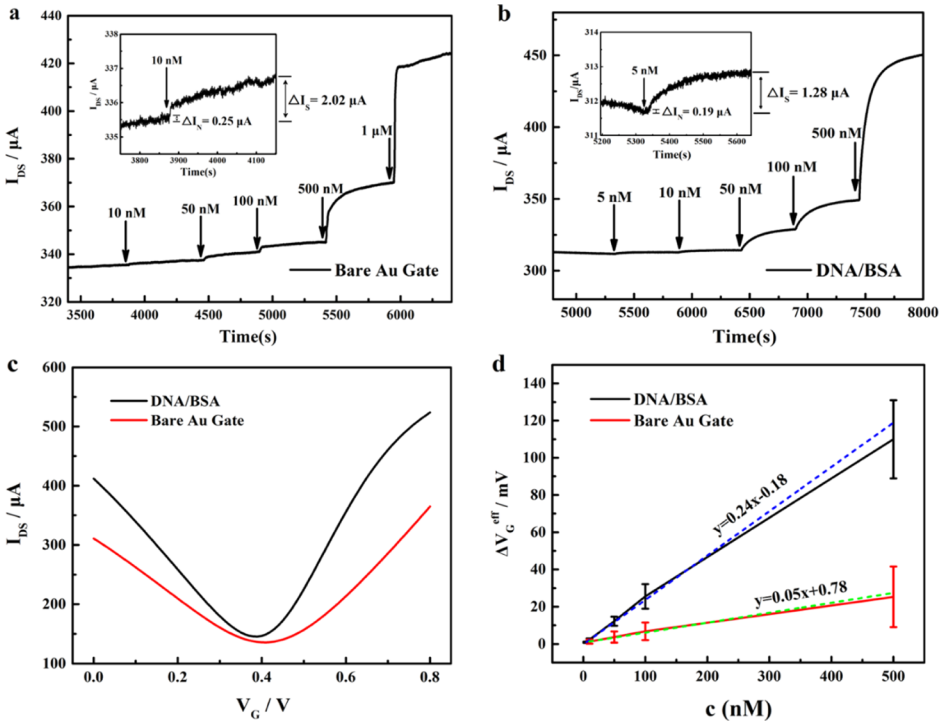

Figure 3. Channel current responses of the (a) SGGT with the bare Au gate and (b) DNA-SGGT with the DNA/BSA-modified gate electrodes to the increasing As(III) concentration in PBS solution measured at fixed V_{DS} = 0.05 V and V_G = 0.7 V. (c) Transfer curves of the SGGT with the bare Au gate (in red) and the DNA-SGGT with the DNA/BSA-modified gate (in black) measured in PBS solution. (d) Calculated effective gate voltage change (ΔV_G^{eff}) of the SGGT with the bare Au gate (in red) and the DNA-SGGT with the DNA/BSA-modified gate as a function of As(III) concentration.

$$I_{DS} \approx \frac{W}{L}\mu C_i |V_G - V_{dirac}| V_{DS} \qquad \text{for } |V_G - V_{dirac}| \gg |V_{DS}| \tag{1}$$

where V_G and V_{DS} are the voltages applied on the gate and the drain, respectively; V_{dirac} is an intrinsic parameter of the SGGT that equals the gate voltage for the charge neutrality point (dirac point) of the graphene channel; W and L are the channel width and length, respectively; μ represents the carrier mobility; and C_i is the gate capacitance. During the actual measurement for real-time channel current, the sensor worked under fixed source−drain voltage V_{DS} = 0.05 V and gate voltage V_G = + 0.7 V. Therefore, as pointed out by eq 1, the channel current I_{DS} is highly dependent on the gate capacitance C_i consisting of two EDL capacitances (C_{G-E} and C_{E-C}), as shown in Figure S2.

It has been reported previously that the SGGT is sensitive to multiple cations due to the potential changes induced by electrochemical reactions at the gate or changes to the electrolyte.[32] However, the SGGT sensor based on this detection mechanism generally lacks selective response to specific cations. To address this problem, we functionalized the gate electrode with DNA probes and then blocked the electrode surface with BSA. Without the presence of As(III), DNA probes were adsorbed onto the gold electrode surface.[43,44] With the addition of As(III), the As(III)/gold interaction is strong enough to affect DNA adsorption and hence change the states of DNA probes on the gate electrode,[43,44] leading to a large redistribution of surface charges and thus the change in gate capacitance C_i. According to eq 1, this will ultimately induce channel current response through field-effect amplification of SGGTs, as also studied in the previous subsection using cDNAs.

As(III) Detection by the SGGT Sensor. In order to evaluate the effectiveness of the DNA-SGGT sensor (i.e., the SGGT with the DNA-modified gate electrode) for detection of As(III), we compared the channel current response of the SGGT sensor with the bare Au gate and that with the modified electrode. For electrochemical sensors, the detection limit is generally determined as the minimum amount of the analyte addition when the corresponding signal-to-noise ratio (S/N) is greater than 3.[48] Figure 3a,b shows the real-time I_{DS} curve of the SGGT toward the continuous addition of As(III), and the insets show the enlarged current response at the detection limit. For the SGGT with the bare Au gate, when 10 nM As(III) was added, the channel current noise ΔI_N was 0.25 μA, while the channel current response ΔI_s was 2.02. The ratio of $\Delta I_s/\Delta I_N$ = 8.08 > 3. Therefore, the detection limit of the SGGT with the bare Au gate for As(III) was determined to be 10 nM or 0.75 μg/kg. Similarly, for the DNA-SGGT, when 5 nM As(III) was added, ΔI_N = 0.19 μA and ΔI_s = 1.28 μA, giving the ratio of $\Delta I_s/\Delta I_N$ = 6.73 > 3. Therefore, the detection limit of the DNA-SGGT for As(III) was 5 nM or 0.375 μg/kg, lower than that of the SGGT with the bare Au gate by twofold. These results indicate that the modification of ssDNA can significantly improve the detection performance of the SGGT sensor for As(III). Figure 3c shows the transfer characteristic curve of the SGGT of the bare Au gate and modified electrode in PBS solution, showing the bipolar characteristics of graphene. The dirac point of the SGGT with the bare Au gate was about 0.41 V, while that of the DNA-SGGT with the DNA/BSA-modified gate was about 0.38 V. The slight left shift of the dirac point indicates that the DNA/BSA modification ultimately led to n-type doping on the graphene channel.

https://dx.doi.org/10.1021/acs.jafc.0c07052
J. Agric. Food Chem. 2021, 69, 1398−1404

The change in effective gate voltage (ΔV_G^{eff}) is regarded as an alternative parameter to evaluate the detection sensitivity of the SGGT sensor. The equivalent gate electrode voltage V_G^{eff} was derived from the transfer characteristic curve of the sensor in blank PBS buffer (Figure 3c) according to channel current I_{DS} values of different As(III) concentrations, as shown in Figure 3a,b. Then, the value of ΔV_G^{eff} as a function of As(III) concentration can be obtained by subtracting the initial equivalent gate voltage value before the addition of As(III). Moreover, the effective voltage change can be fitted with the equations given by[49]

$$V_G^{eff} = V_{G-E} + V_{E-C} = \frac{Q}{C_{G-E}} + V_{E-C} = \frac{4\pi kd\rho}{\varepsilon_0 \varepsilon_r} + V_{E-C} \quad (2)$$

where ε_0 is the electric permittivity constant, ε_r is the relative electric permittivity, ρ is the surface charge density, and d is the EDL thickness. According to the sensing mechanism discussed in the previous subsection, the adsorption of DNA probes on the Au gate electrode was disrupted by the As(III)/Au interactions, causing larger separation of negative charges of DNA probes from the gate. Therefore, by rough estimation, d in eq 2 is proportional to the As(III) concentration, namely

$$\Delta V_G^{eff} = \alpha C_{As(III)} + C \quad (3)$$

where C is a constant and α is the slope of V_G^{eff} per As(III) concentration ($C_{As(III)}$). Equation 3 indicates that the equivalent gate voltage (V_G^{eff}) shifts to a larger value with the increase in As(III) concentration. In addition, the channel current I_{DS} also increased with the increase in V_G^{eff} when the DNA-SGGT sensor worked in the n-type region ($V_G = 0.7$ V > V_{dirac}).

Figure 3d shows the computed effective gate voltage change (ΔV_G^{eff}) as a function of As(III) concentration. We found that there was a clear linear relationship between the ΔV_G^{eff} and As(III) concentration. The slope generally represents the sensitivity of the sensor. It was derived that the DNA-SGGT sensor with the modified gate had a slope value of 0.24 mV/nM, significantly higher than the value of the SGGT sensor with the bare Au gate (0.05 mV/nM).

Selective Test. The main purpose of the DNA/BSA functionalization was to improve the selective responses to the As(III) target. For characterization of selectivity, the specificity test was performed by computing the effective gate voltage change (ΔV_G^{eff}) from measured real-time channel current to other interfering metal ions at even much higher concentration (10 μM), including K^+, Pb^{2+}, Co^{2+}, Cu^{2+}, Ni^{2+}, Fe^{3+}, Cr^{3+}, Mn^{2+}, Cd^{2+}, Na^+, Mg^{2+}, Zn^{2+}, Ba^{2+}, Ca^{2+}, Se^{4+}, Sb^{3+}, and Al^{3+}. The red bars in Figure 4 represent the responses of the SGGT sensor with the bare Au gate to these ions. It can be seen that some other metal ions (such as Co^{2+}, Cu^{2+}, Ni^{2+}, Fe^{3+}, Cr^{3+}, and Mn^{2+}) also caused comparable or even larger responses as 500 nM As(III) (i.e., 25.29 mV) for the SGGT sensor with the bare Au gate. In contrast, the black bars in Figure 4 show the responses of the DNA-SGGT sensor with the DNA/BSA-modified gate. It was observed that 500 nM As(III) induced the highest response with a ΔV_G^{eff} value of 109.92 ± 21.08 mV. The response to other interferences was weak at 10 μM, and the ΔV_G^{eff} values of K^+ (0.76 ± 0.45 mV), Pb^{2+} (2.82 ± 0.01 mV), Co^{2+} (5.76 ± 0.19 mV), Cu^{2+} (18.38 ± 8.32 mV), Ni^{2+} (23.01 ± 7.95 mV), Fe^{3+} (17.84 ± 0.49 mV), Cr^{3+} (4.05 ± 2.82 mV), Mn^{2+} (2.90 ± 0.45 mV), Cd^{2+} (4.83 ± 2.90 mV), Na^+ (0.50 ± 0.12 mV), Mg^{2+} (3.02 ± 1.57 mV), Zn^{2+} (8.86 ± 4.99 mV), Ba^{2+} (3.59 ± 0.80 mV), Ca^{2+} (4.13 ± 1.49 mV), Se^{4+} (−5.90 ± 0.40 mV), Sb^{3+} (−22.63 ± 2.85 mV), and Al^{3+} (1.21 ± 0.18 mV) were significantly lower than that of As(III) at 500 nM. These results clearly suggest that the DNA/BSA functionalization to the gate electrode dramatically reduced the response of the sensor to the many interfering metal ions, for example, the response to Mn^{2+} was lowered by nearly 98 times. In the meanwhile, the response of the DNA-SGGT with the DNA/BSA-modified gate was enhanced by more than fourfold than that of the SGGT with the bare Au gate. Therefore, it can be concluded that DNA/BSA functionalization to the gate electrode effectively improved the selective response of the sensor to target As(III) ions.

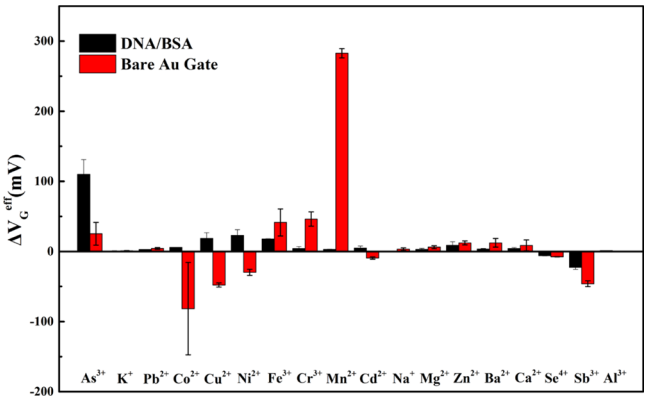

Figure 4. Selectivity measurements of the SGGT with the bare Au gate (red bars) and the DNA-SGGT with the DNA/BSA-modified gate (black bars). The ΔV_G^{eff} signal responses of the sensor to target As(III) at 500 nM and other interfering cations at 10 μM, including K^+, Pb^{2+}, Co^{2+}, Cu^{2+}, Ni^{2+}, Fe^{3+}, Cr^{3+}, Mn^{2+}, Cd^{2+}, Na^+, Mg^{2+}, Zn^{2+}, Ba^{2+}, Ca^{2+}, Se^{4+}, Sb^{3+}, and Al^{3+}, were calculated. Error bars represent the standard deviation of three independent repeated experiments.

Real Sample Testing. Ultimately, we applied the DNA-SGGT-based sensor for detection of As(III) in rice samples. First, we grinded the arsenic-free rice from the market into powder and added As_2O_3 to the crushed rice sample and stirred well. Then, an appropriate amount of DI water and NaOH were added so that a weak alkaline mixed solution of 100 nM (i.e., 7.5 μg/kg) concentration of As(III) ion and rice was prepared. The mixture was centrifuged, and the supernatant was collected for subsequent measurements.

The DNA-SGGT-based sensor was calibrated in PBS solution in order to obtain the relationship between As(III) concentration and the equivalent gate voltage change ΔV_G^{eff} (i.e., standard curve). Then, the prepared As(III)-spiked rice sample was applied to the optimized DNA-SGGT-based sensor in 10 μL volume, and the results are shown in Figure 5. The V_G^{eff} value corresponding to channel current I_{DS} before the addition of the aqueous rice sample was called the initial equivalent gate voltage (i.e., baseline). By subtracting the initial equivalent gate voltage value, the equivalent gate electrode voltage change value ΔV_G^{eff} corresponding to the 10 μL rice sample was obtained. The As(III) concentration in the rice sample was calculated by substituting the corresponding effective gate voltage change into the standard curve.[50] In this manner, the concentration of As(III) in the spiked rice sample was computed to be 93.55 ± 10.69 nM (i.e., 7.02 μg/kg) and the recovery was thus determined to be 93.55%. Through modification of the gate electrode with other target-

https://dx.doi.org/10.1021/acs.jafc.0c07052
J. Agric. Food Chem. 2021, 69, 1398−1404

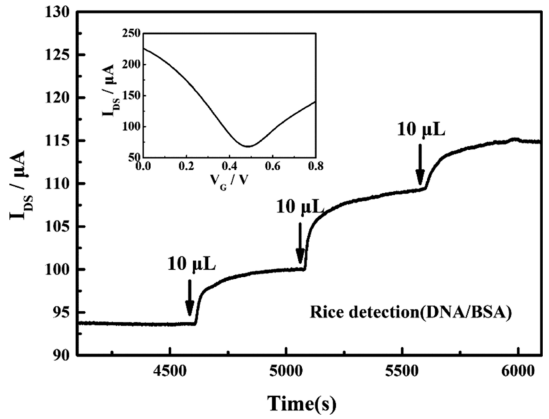

Figure 5. Real-time channel current responses of the DNA-SGGT-based As(III) sensor to three continuous additions of 10 μL rice samples spiked with 100 nM (i.e., 7.5 μg/kg) As(III). The recovery rate of the sensor for real rice samples is calculated based on the triple measurements. Inset: transfer curve of the sensor measured in PBS solution.

specific DNA probes (such as aptamers and DNAzymes), the DNA-SGGT-based sensor provides a promising electrochemical biosensing platform for fast on-site detection of heavy metal ions in many types of food samples with high sensitivity, selectivity, and accuracy.

■ ASSOCIATED CONTENT

Supporting Information

The Supporting Information is available free of charge at https://pubs.acs.org/doi/10.1021/acs.jafc.0c07052.

Additional figures and tables for an actual picture of the DNA-SGGT-based As(III) sensor, sketch for the potential drops on the EDL of the sensor, sketch for detection of complementary DNA strands (cDNAs) using the DNA-SGGT, results of the anti-interference measurements for the DNA-SGGT sensor, list of the sequences and modifications of the DNA strands, and comparison of As(III) detection using the DNA-SGGT sensor and other fast detecting methods (PDF)

■ AUTHOR INFORMATION

Corresponding Author

Hao Qu − *School of Food and Biological Engineering, Hefei University of Technology, Hefei 230009, China;* orcid.org/0000-0002-5834-8080; Email: quhao@hfut.edu.cn

Authors

Yuhong Wang − *School of Food and Biological Engineering, Hefei University of Technology, Hefei 230009, China*

Yulong Bi − *School of Food and Biological Engineering, Hefei University of Technology, Hefei 230009, China*

Rongrong Wang − *School of Food and Biological Engineering, Hefei University of Technology, Hefei 230009, China*

Lu Wang − *School of Food and Biological Engineering, Hefei University of Technology, Hefei 230009, China*

Lei Zheng − *School of Food and Biological Engineering and Intelligent Interconnected Systems Laboratory of Anhui Province, Hefei University of Technology, Hefei 230009, China;* orcid.org/0000-0001-8367-5502

Complete contact information is available at: https://pubs.acs.org/10.1021/acs.jafc.0c07052

Notes

The authors declare no competing financial interest.

■ ACKNOWLEDGMENTS

This study was supported by the National Key Research and Development Plan of China (2017YFC1600603), the National Natural Science Foundation of China (21705031 and 31901406), the Key Science & Technology Specific Projects of Anhui Province (202003a06020017 and 18030701200), and the Fundamental Research Funds for the Central Universities (JZ2020HGTB0044 and JZ2019HGBH0196).

■ REFERENCES

(1) Batten, M. L.; Imanishi, Y.; Tu, D. C.; Doan, T.; Zhu, L.; Pang, J.; Glushakova, L.; Moise, A. R.; Baehr, W.; Van Gelder, R. N.; Hauswirth, W. W.; Rieke, F.; Palczewski, K. Pharmacological and rAAV Gene Therapy Rescue of Visual Functions in a Blind Mouse Model of Leber Congenital Amaurosis. *PLoS Med.* **2005**, *2*, No. e333.

(2) Norton, G. J.; Pinson, S. R. M.; Alexander, J.; McKay, S.; Hansen, H.; Duan, G.-L.; Rafiqul Islam, M.; Islam, S.; Stroud, J. L.; Zhao, F.-J.; McGrath, S. P.; Zhu, Y.-G.; Lahner, B.; Yakubova, E.; Guerinot, M. L.; Tarpley, L.; Eizenga, G. C.; Salt, D. E.; Meharg, A. A.; Price, A. H. Variation in Grain Arsenic Assessed in a Diverse Panel of Rice (*Oryza Sativa*) Grown in Multiple Sites. *New Phytol.* **2012**, *193*, 650−664.

(3) Su, Y.-H.; McGrath, S. P.; Zhao, F.-J. Rice is More Efficient in Arsenite Uptake and Translocation than Wheat and Barley. *Plant Soil* **2010**, *328*, 27−34.

(4) Huang, Y.; Wang, M.; Mao, X.; Qian, Y.; Chen, T.; Zhang, Y. Concentrations of Inorganic Arsenic in Milled Rice from China and Associated Dietary Exposure Assessment. *J. Agric. Food Chem.* **2015**, *63*, 10838−10845.

(5) Hettick, B. E.; Cañas-Carrell, J. E.; French, A. D.; Klein, D. M. Arsenic: A Review of the Element's Toxicity, Plant Interactions, and Potential Methods of Remediation. *J. Agric. Food Chem.* **2015**, *63*, 7097−7107.

(6) Li, G.; Sun, G.-X.; Williams, P. N.; Nunes, L.; Zhu, Y.-G. Inorganic Arsenic in Chinese Food and Its Cancer Risk. *Environ. Int.* **2011**, *37*, 1219−1225.

(7) Bradham, K.; Herde, C.; Herde, P.; Juhasz, A. L.; Herbin-Davis, K.; Elek, B.; Farthing, A.; Diamond, G. L.; Thomas, D. J. Intra- and Interlaboratory Evaluation of an Assay of Soil Arsenic Relative Bioavailability in Mice. *J. Agric. Food Chem.* **2020**, *68*, 2615−2622.

(8) Lewchalermvong, K.; Rangkadilok, N.; Nookabkaew, S.; Suriyo, T.; Satayavivad, J. Arsenic Speciation and Accumulation in Selected Organs after Oral Administration of Rice Extracts in Wistar Rats. *J. Agric. Food Chem.* **2018**, *66*, 3199−3209.

(9) Han, Y.-H.; Liu, X.; Rathinasabapathi, B.; Li, H.-B.; Chen, Y.; Ma, L. Q. Mechanisms of Efficient As Solubilization in Soils and As Accumulation by As-Hyperaccumulator *Pteris Vittata*. *Environ. Pollut.* **2017**, *227*, 569−577.

(10) Wang, Y.; Wang, S.; Xu, P.; Liu, C.; Liu, M.; Wang, Y.; Wang, C.; Zhang, C.; Ge, Y. Review of Arsenic Speciation, Toxicity and Metabolism in Microalgae. *Rev. Environ. Sci. Bio/Technol.* **2015**, *14*, 427−451.

(11) Wang, X.; Geng, A.; Dong, Y.; Fu, C.; Li, H.; Zhao, Y.; Li, Q. X.; Wang, F. Comparison of Translocation and Transformation from Soil to Rice and Metabolism in Rats for Four Arsenic Species. *J. Agric. Food Chem.* **2017**, *65*, 8992−8998.

(12) Wu, Y.; Liu, L.; Zhan, S.; Wang, F.; Zhou, P. Ultrasensitive Aptamer Biosensor for Arsenic(III) Detection in Aqueous Solution Based on Surfactant-Induced Aggregation of Gold Nanoparticles. *Analyst* **2012**, *137*, 4171−4178.

(13) Mays, D. E.; Hussam, A. Voltammetric methods for determination and speciation of inorganic arsenic in the environment-A review. *Anal. Chim. Acta* **2009**, *646*, 6−16.
(14) Cao, X.; Hao, C.; Wang, G.; Yang, H.; Chen, D.; Wang, X. Sequential extraction combined with HPLC-ICP-MS for As speciation in dry seafood products. *Food Chem.* **2009**, *113*, 720−726.
(15) Narukawa, T.; Chiba, K.; Sinaviwat, S.; Feldmann, J. A Rapid Monitoring Method for Inorganic Arsenic in Rice Flour Using Reversed Phase-High Performance Liquid Chromatography-Inductively Coupled Plasma Mass Spectrometry. *J. Chromatogr. A* **2017**, *1479*, 129−136.
(16) Narukawa, T.; Inagaki, K.; Kuroiwa, T.; Chiba, K. The extraction and speciation of arsenic in rice flour by HPLC-ICP-MS. *Talanta* **2008**, *77*, 427−432.
(17) Signes-Pastor, A. J.; Carey, M.; Meharg, A. A. Inorganic Arsenic Removal in Rice Bran by Percolating Cooking Water. *Food Chem.* **2017**, *234*, 76−80.
(18) Richter, J.; Lischka, S.; Piechotta, C. Analysis of arsenic species in fish after derivatization by GC-MS. *Talanta* **2012**, *101*, 524−529.
(19) Qu, H.; Mudalige, T. K.; Linder, S. W. Arsenic Speciation in Rice by Capillary Electrophoresis/Inductively Coupled Plasma Mass Spectrometry: Enzyme-Assisted Water-Phase Microwave Digestion. *J. Agric. Food Chem.* **2015**, *63*, 3153−3160.
(20) Shi, G. L.; Zhu, S.; Bai, S. N.; Xia, Y.; Lou, L. Q.; Cai, Q. S. The Transportation and Accumulation of Arsenic, Cadmium, and Phosphorus in 12 Wheat Cultivars and Their Relationships with Each Other. *J. Hazard Mater.* **2015**, *299*, 94−102.
(21) Wang, Y.; Zhang, C.; Zheng, Y.; Ge, Y. Bioaccumulation Kinetics of Arsenite and Arsenate in Dunaliella Salina Under Different Phosphate Regimes. *Environ. Sci. Pollut. Res.* **2017**, *24*, 21213−21221.
(22) Musil, S.; Pétursdóttir, Á. H.; Raab, A.; Gunnlaugsdóttir, H.; Krupp, E.; Feldmann, J. Speciation Without Chromatography Using Selective Hydride Generation: Inorganic Arsenic in Rice and Samples of Marine Origin. *Anal. Chem.* **2014**, *86*, 993−999.
(23) Ezeh, V. C.; Harrop, T. C. A Sensitive and Selective Fluorescence Sensor for the Detection of Arsenic(III) in Organic Media. *Inorg. Chem.* **2012**, *51*, 1213−1215.
(24) Mulvihill, M.; Tao, A.; Benjauthrit, K.; Arnold, J.; Yang, P. Surface-Enhanced Raman Spectroscopy for Trace Arsenic Detection in Contaminated Water. *Angew. Chem., Int. Ed.* **2008**, *47*, 6456−6460.
(25) Forzani, E. S.; Foley, K.; Westerhoff, P.; Tao, N. Detection of Arsenic in Groundwater Using a Surface Plasmon Resonance Sensor. *Sens. Actuators, B* **2007**, *123*, 82−88.
(26) Trang, P. T. K.; Berg, M.; Viet, P. H.; Mui, N. V.; van der Meer, J. R. Bacterial Bioassay for Rapid and Accurate Analysis of Arsenic in Highly Variable Groundwater Samples. *Environ. Sci. Technol.* **2005**, *39*, 7625−7630.
(27) Guo, Z.; Yang, M.; Huang, X.-J. Recent Developments in Electrochemical Determination of Arsenic. *Curr. Opin. Electrochem.* **2017**, *3*, 130−136.
(28) Geim, A. K. Random Walk to Graphene (Nobel Lecture). *Angew. Chem., Int. Ed.* **2011**, *50*, 6966−6985.
(29) Novoselov, K. S.; Geim, A. K.; Morozov, S. V.; Jiang, D.; Zhang, Y.; Dubonos, S. V.; Grigorieva, I. V.; Firsov, A. A. Electric Field Effect in Atomically Thin Carbon Films. *Science* **2004**, *306*, 666.
(30) Justino, C. I. L.; Gomes, A. R.; Freitas, A. C.; Duarte, A. C.; Rocha-Santos, T. A. P. Graphene Based Sensors and Biosensors. *Trac. Trends Anal. Chem.* **2017**, *91*, 53−66.
(31) Thanh, T. D.; Balamurugan, J.; Lee, S. H.; Kim, N. H.; Lee, J. H. Effective Seed-Assisted Synthesis of Gold Nanoparticles Anchored Nitrogen-Doped Graphene for Electrochemical Detection of Glucose and Dopamine. *Biosens. Bioelectron.* **2016**, *81*, 259−267.
(32) Yan, F.; Zhang, M.; Li, J. Solution-Gated Graphene Transistors for Chemical and Biological Sensors. *Adv. Healthcare Mater.* **2014**, *3*, 313−331.
(33) Dong, X.; Shi, Y.; Huang, W.; Chen, P.; Li, L.-J. Electrical Detection of DNA Hybridization with Single-Base Specificity Using Transistors Based on CVD-Grown Graphene Sheets. *Adv. Mater.* **2010**, *22*, 1649−1653.
(34) Ohno, Y.; Maehashi, K.; Matsumoto, K. Chemical and Biological Sensing Applications Based on Graphene Field-Effect Transistors. *Biosens. Bioelectron.* **2010**, *26*, 1727−1730.
(35) Kwak, Y. H.; Choi, D. S.; Kim, Y. N.; Kim, H.; Yoon, D. H.; Ahn, S.-S.; Yang, J.-W.; Yang, W. S.; Seo, S. Flexible Glucose Sensor Using CVD-Grown Graphene-Based Field Effect Transistor. *Biosens. Bioelectron.* **2012**, *37*, 82−87.
(36) He, R. X.; Lin, P.; Liu, Z. K.; Zhu, H. W.; Zhao, X. Z.; Chan, H. L. W.; Yan, F. Solution-Gated Graphene Field Effect Transistors Integrated in Microfluidic Systems and Used for Flow Velocity Detection. *Nano Lett.* **2012**, *12*, 1404−1409.
(37) Newaz, A. K. M.; Markov, D. A.; Prasai, D.; Bolotin, K. I. Graphene Transistor as a Probe for Streaming Potential. *Nano Lett.* **2012**, *12*, 2931−2935.
(38) Xiong, C.; Zhang, T.; Wang, D.; Lin, Y.; Qu, H.; Chen, W.; Luo, L.; Wang, Y.; Zheng, L.; Fu, L. Highly Sensitive Solution-Gated Graphene Transistor Based Sensor for Continuous and Real-Time Detection of Free Chlorine. *Anal. Chim. Acta* **2018**, *1033*, 65−72.
(39) Wang, R.; Mao, Y.; Qu, H.; Chen, W.; Ma, A.; Zheng, L. Highly Sensitive and Selective Sulfite Sensors Based on Solution-Gated Graphene Transistors with Multi-Walled Carbon Nanotube Functionalized Gate Electrodes. *Food Chem.* **2019**, *290*, 101−106.
(40) Gao, S.; Wang, R.; Bi, Y.; Qu, H.; Chen, Y.; Zheng, L. Identification of Frozen/Thawed Beef Based on Label-Free Detection of Hemin (Iron Porphyrin) with Solution-Gated Graphene Transistor Sensors. *Sens. Actuators, B* **2020**, *305*, 127167.
(41) Heller, I.; Chatoor, S.; Männik, J.; Zevenbergen, M. A. G.; Dekker, C.; Lemay, S. G. Influence of Electrolyte Composition on Liquid-Gated Carbon Nanotube and Graphene Transistors. *J. Am. Chem. Soc.* **2010**, *132*, 17149−17156.
(42) Chen, F.; Qing, Q.; Xia, J.; Li, J.; Tao, N. Electrochemical Gate-Controlled Charge Transport in Graphene in Ionic Liquid and Aqueous Solution. *J. Am. Chem. Soc.* **2009**, *131*, 9908−9909.
(43) Zong, C.; Liu, J. The Arsenic-Binding Aptamer Cannot Bind Arsenic: Critical Evaluation of Aptamer Selection and Binding. *Anal. Chem.* **2019**, *91*, 10887−10893.
(44) Zong, C.; Zhang, Z.; Liu, B.; Liu, J. Adsorption of Arsenite on Gold Nanoparticles Studied with DNA Oligonucleotide Probes. *Langmuir* **2019**, *35*, 7304−7311.
(45) Wen, Y.; Li, F. Y.; Dong, X.; Zhang, J.; Xiong, Q.; Chen, P. The Electrical Detection of Lead Ions Using Gold-Nanoparticle- and DNAzyme-Functionalized Graphene Device. *Adv. Healthcare Mater.* **2013**, *2*, 271−274.
(46) Zheng, W.; Teng, J.; Cheng, L.; Ye, Y.; Pan, D.; Wu, J.; Xue, F.; Liu, G.; Chen, W. Hetero-Enzyme-Based Two-Round Signal Amplification Strategy for Trace Detection of Aflatoxin B1 Using an Electrochemical Aptasensor. *Biosens. Bioelectron.* **2016**, *80*, 574−581.
(47) Chen, F.; Qing, Q.; Xia, J.; Tao, N. Graphene Field-Effect Transistors: Electrochemical Gating, Interfacial Capacitance, and Biosensing Applications. *Chem.−Asian J.* **2010**, *5*, 2144−2153.
(48) Liao, C.; Zhang, M.; Niu, L.; Zheng, Z.; Yan, F. Organic Electrochemical Transistors with Graphene-Modified Gate Electrodes for Highly Sensitive and Selective Dopamine Sensors. *J. Mater. Chem. B* **2014**, *2*, 191−200.
(49) Zhang, M.; Liao, C.; Mak, C. H.; You, P.; Mak, C. L.; Yan, F. Highly Sensitive Glucose Sensors Based on Enzyme-Modified Whole-Graphene Solution-Gated Transistors. *Sci. Rep.* **2015**, *5*, 8311.
(50) Xiong, C.; Zhang, T.; Kong, W.; Zhang, Z.; Qu, H.; Chen, W.; Wang, Y.; Luo, L.; Zheng, L. ZIF-67 Derived Porous Co3O4 Hollow Nanopolyhedron Functionalized Solution-Gated Graphene Transistors for Simultaneous Detection of Glucose and Uric Acid in Tears. *Biosens. Bioelectron.* **2018**, *101*, 21−28.

https://dx.doi.org/10.1021/acs.jafc.0c07052
J. Agric. Food Chem. 2021, 69, 1398−1404